Electronic Supplementary Information

Assessing the relevance of building block crystallinity for tuning the stiffness of gold nanocrystal superlattices

Cong Yan, Hervé Portalès, Nicolas Goubet, Imad Arfaoui, Sergey Sirotkin, Alain Mermet and Marie-Paule Pileni

1. Synthesis of Au nanocrystals

For the synthesis of Au nanocrystals used in this work, typically (PPh3)Au−Cl molecules are dissolved in toluene with the protection of nitrogen. Then the solution is heated to 100 °C, and a certain amount of dodecanethiol is added with a vigorous stirring. Meanwhile, amine−borane complex is dissolved in toluene as the reductive solution, which is also heated to 100 °C. When both solutions are stabilized, they are mixed together to form the gold NCs and the color of mixture solution will turn to dark red. The Au nanocrystals size is controlled by changing the amount of dodecanethiol and the coating agents. The NCs can be redispersed in toluene to self-assemble.

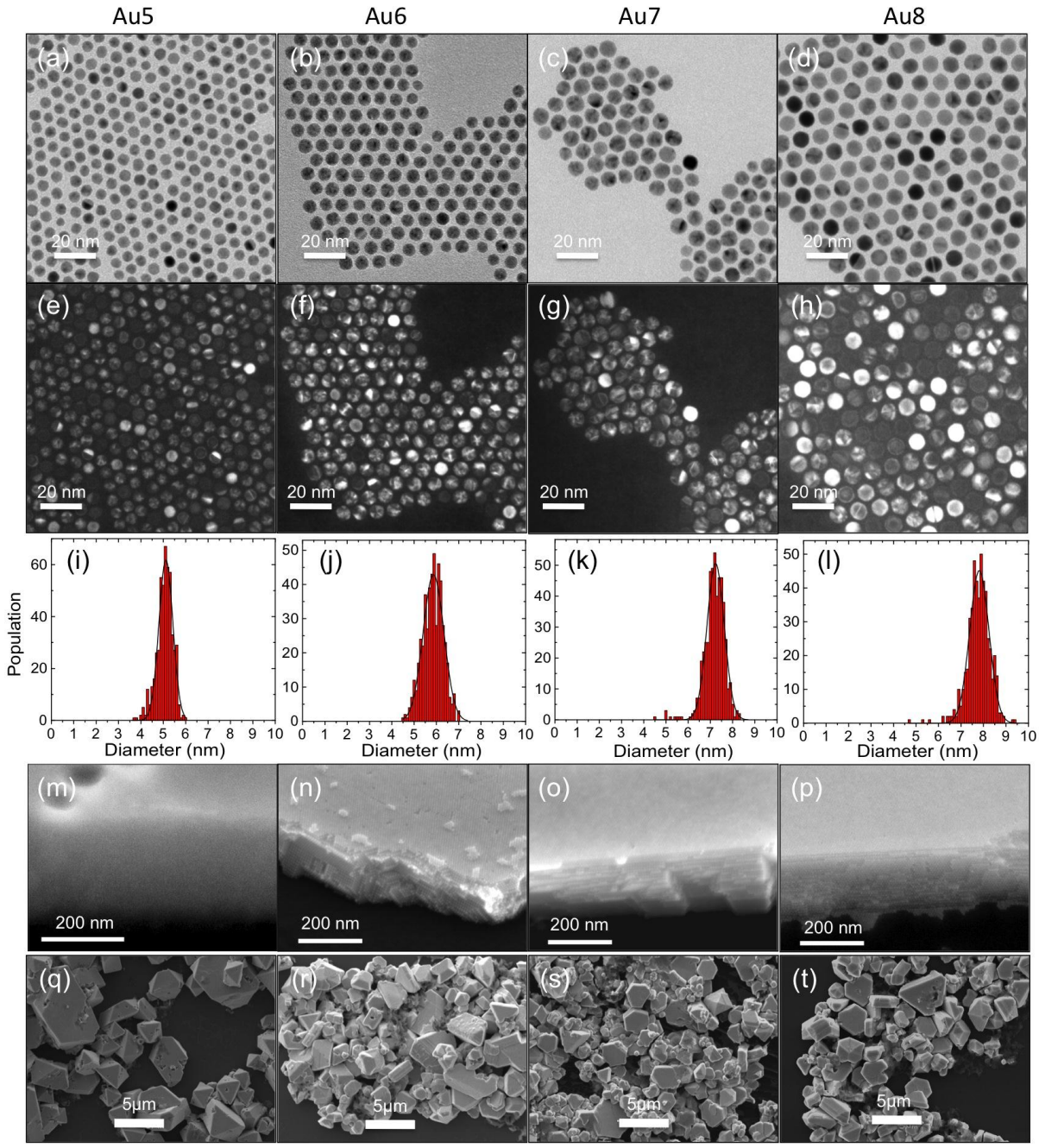

Fig. S1 TEM bright field (a)-(d) and dark field (e)-(h) images of Au NCs with size of 5, 6, 7 and 8 nm, respectively. (i)-(l) histograms show narrow NC size dispersion. (m)-(p) HRSEM images of interfacial supracrystals with different NC sizes. (q)-(t) SEM images of precipitated supracrystals with different NC sizes.

2. Oliver and Pharr's model

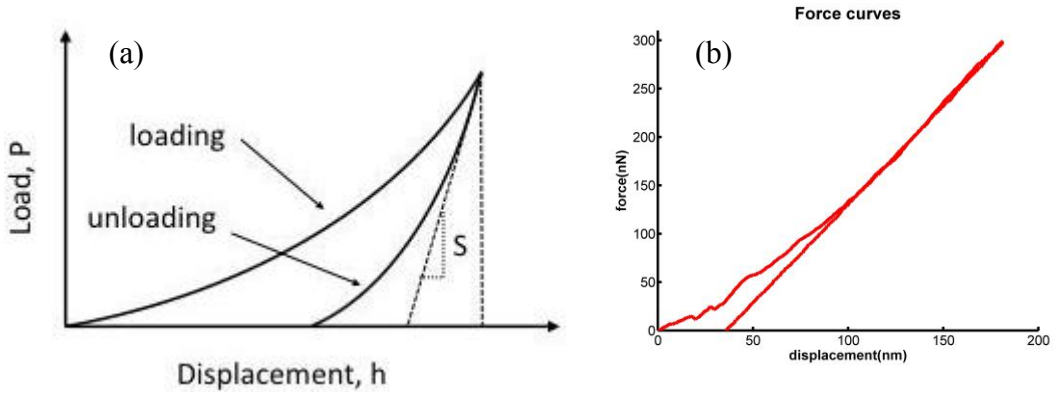

Fig. S2 (a) Schematic illustration of loading and unloading curves and (b) the force curve obtained from the AFM nanoindentation measurements.

In this model, it is assumed that the uploading data arise from a pure elastic contact and it follows the equations below:

$$E = \frac{\sqrt{\pi}}{2}\frac{S}{\sqrt{A}} \tag{1}$$

where E is the Young's modulus, A is the contact area and S is the experimentally measured contact stiffness, defined as:

$$S = \frac{dP}{dh} \tag{2}$$

where P is the loading force and h is the elastic displacement.

Here, the value of E for each sample is obtained by using the commercial software "Punias" which reads the original data, *i.e.* the load-displacement curves and calculates the Young's modulus by extracting the force versus penetration (P-h) curve. After each sets of measurements, the cantilever is calibrated with mica substrate in order to obtain the up-to-date parameters of the cantilever for the elastic modulus calculation. A thermal K card is used to deduce the proper stiffness of the cantilever. For the contact area between the tip and the sample: (i) the manufacture's specifications of the tip were taken into account; (ii) the shape of the AFM probe

was checked by SEM; (iii) the value of the contact area is verified by measuring the Young's modulus of a reference sample as a Teflon foil. It should be mentioned here that for the measurement of the Au_5 multiple twinned particles (MTPs), a softer AFM probe with spring constant of 0.08 N/m was used because the standard 4.5 N/m AFM tips drastically damage this particular sample.

3. Plate model

The plate model treats the interfacial supracrystal films at a flat circular plate of constant thickness. The indentation of AFM tip was modeled as a uniform load over a very small central circular area while the edge of the plate (the interfacial films) is simply supported. A schematic illustration is given in Figure S3.

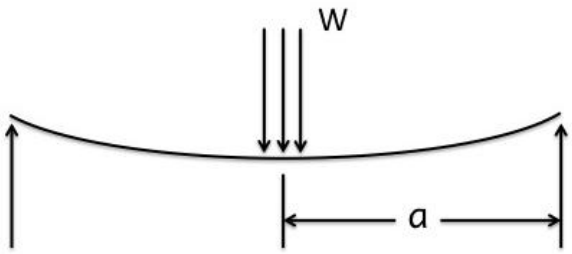

Fig. S3 Schematic illustration of the plate model where *W* is the total applied force and *a* is the radius of the plate.

In such case, the displacement *y* of the central point could be expressed as:

$$y = \frac{Wa^2}{16\pi D}\frac{3+\nu}{1+\nu} \tag{3}$$

and

$$D = \frac{Et^3}{12(1-\nu^2)} \tag{4}$$

where *t* is the thickness of the plate and *v* is the Poisson ratio. In this work, the loading force is obtained by the AFM measurements directly and displacement of the central point was calculated by:

$$y = h_p - h_i - h_r \tag{5}$$

where h_p is the displacement of the piezomotor, h_i is the indentation depth which measured by AFM profile, and h_r is the deflection of the cantilever. Thus the Young's modulus E could be calculated through equations (3)-(5) when y is obtained.

4. Residual Marks

In the measurements for both interfacial and precipitated supracrystals, AFM images are recorded before and after the indentation to track the indentation marks. Following show the residual marks for both interfacial and precipitated supracrystals.

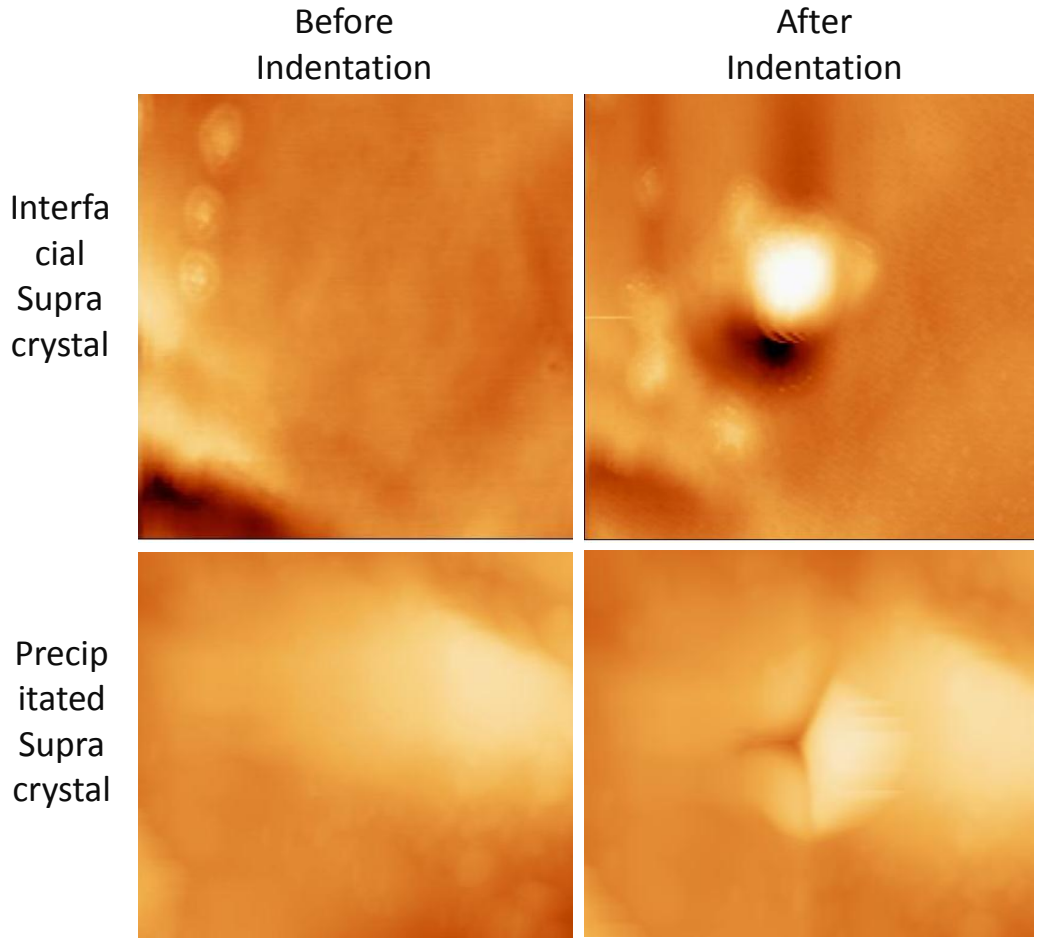

Fig. S4 AFM images recorded the residual marks after the indentation for both interfacial and precipitated supracrystals.

5. Electron diffraction of single domain and polycrystalline NCs

In the inset of Figure S5a, it shows the low-angle electron diffraction pattern of single Au NCs films with hexagonal symmetry, which confirms the compact structure of the NC superlattice. The high-angle diffraction pattern presented in Figure S5a exhibits several rings corresponding to electron diffraction by specific planes of atomic lattices with fcc structure. Such feature provides evidence for an average coherent alignment of the atomic lattice planes of NCs to one another within the superlattice. In contrast, Figure S5b shows the high-angle diffraction pattern obtained from polycrystalline NCs, in which diffraction rings exhibit no similar arcs as those previously mentioned although these NCs are also close-packed in compact superlattice, as shown by the inset in Figure S5b. This result means that polycrystalline NCs self-assemble into arrays with long-range translational but no orientational ordering.

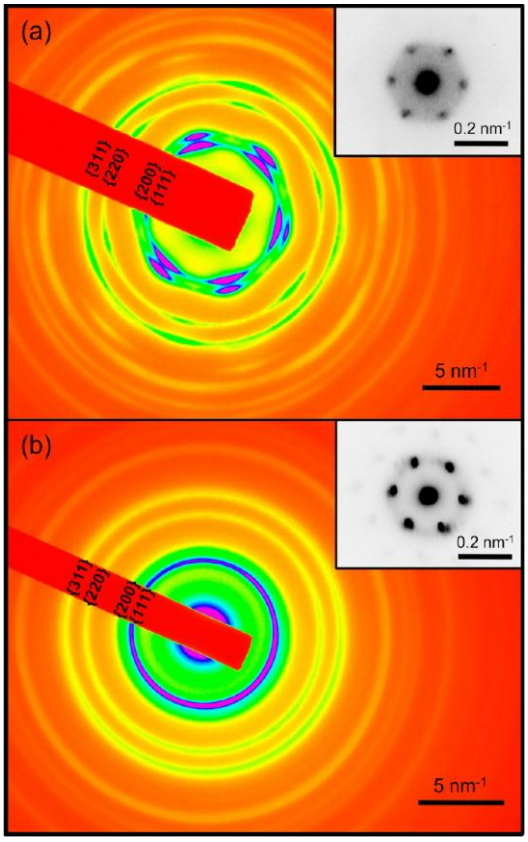

Fig. S5 High-angle electron diffraction patterns recorded from a thin film of close-packed (a) single crystalline and (b) polycrystalline Au NCs. Insets in (a) and (b) show the low-angle electron diffraction patterns recorded from self-assembled single crystalline and polycrystalline Au NCs, respectively. Reproduced from reference **26**